Asian Journal of Current Research in Clinical Cancer
ISSN: 3062-4444
2025, Volume 5, Issue 2, Page No: 106-117

Available online at: www.galaxypub.co/page/journals

Galaxy Publication

Deep Learning-Estimated T2 Mapping Enhances Radiomics-Based Detection of Clinically Significant Peripheral Zone Prostate Cancer

Christopher S. Allen[1]*, Rebecca M. Boyd[1], Jonathan P. Greene[1]

[1]Department of Radiation Oncology, Harvard Medical School, Boston, MA, USA.

***E-mail** ✉ chris.allen.science@protonmail.com

Received: 16 August 2025; **Revised:** 15 October 2025; **Accepted:** 17 October 2025

ABSTRACT

Abstract

Multiparametric MRI (mpMRI) is a key, non-invasive imaging approach used to identify and localize prostate cancer (PCa). When integrated with radiomic feature extraction, mpMRI data can assist in estimating tumor aggressiveness. Although T2 mapping delivers quantitative metrics useful for PCa assessment, it is not yet routinely implemented in clinical imaging workflows. Our team previously introduced a deep learning framework capable of generating estimated T2 maps from standard T1- and T2-weighted sequences. This study explores the incremental diagnostic benefit of incorporating those estimated T2 maps with conventional T2-weighted scans for identifying clinically significant prostate cancer (csPCa). A total of 76 peripheral zone lesions, covering both clinically significant and insignificant PCa cases, were retrospectively assessed. Radiomic features were obtained from standard T2-weighted scans and the AI-generated T2 maps. Feature selection and model development were performed using five-fold cross-validation. Logistic regression and Gaussian Process classifiers were applied, and diagnostic performance was evaluated through area under the curve (AUC) and accuracy metrics. The combined approach using both T2-weighted and estimated T2 map features achieved an AUC of 0.803, which was significantly higher than that obtained from models using only T2-weighted features (AUC = 0.700, p = 0.048). Deep learning-based T2 map features offer complementary quantitative data that enhance the prediction accuracy for peripheral zone csPCa, supporting improved risk evaluation in non-invasive prostate cancer diagnostics.

Keywords: Prostate cancer, Clinically significant, mpMRI, T2 mapping, Radiomics, Quantitative imaging, Machine learning, Peripheral zone

How to Cite This Article: Allen CS, Boyd RM, Greene JP. Deep Learning-Estimated T2 Mapping Enhances Radiomics-Based Detection of Clinically Significant Peripheral Zone Prostate Cancer. Asian J Curr Res Clin Cancer. 2025;5(2):106-17. https://doi.org/10.51847/Zbi00848kx

Introduction

Prostate cancer (PCa) remains the most commonly diagnosed malignancy in men, with about 299, 010 new diagnoses and 35, 250 related deaths projected in the United States for 2024 [1, 2]. Accurate identification and timely management of clinically significant PCa (csPCa) are essential for improving therapeutic outcomes [3].

Conventional PCa evaluation methods typically include prostate-specific antigen (PSA) screening, digital rectal examination (DRE), and transrectal ultrasound (TRUS)-guided biopsy. These approaches, however, often yield high false-positive and false-negative results in PCa detection [4, 5], and biopsies introduce procedural risks, potential complications, and sampling bias [6, 7].

To address these issues, multiparametric MRI (mpMRI) has become an established, non-invasive imaging modality for prostate lesion detection and localization. With the guidance of the Prostate Imaging Reporting and Data System (PI-RADS) v2.1 [8], mpMRI combines structural and functional imaging data, improving csPCa diagnostic precision and minimizing both overdiagnosis and unnecessary treatment [9-12]. Yet, interpreting mpMRI results requires extensive expertise, and consistency between readers remains moderate [13, 14].

Radiomics has emerged as a data-driven technique for enhancing diagnostic precision [15, 16]. By converting imaging data into high-dimensional features and applying machine learning, radiomics can characterize PCa

aggressiveness [17-20]. Among mpMRI components, T2-weighted imaging is particularly informative, though it provides relative signal intensity that can fluctuate with scanners and acquisition settings.

Quantitative T2 mapping, which directly measures intrinsic tissue parameters, has shown strong reproducibility and reduced dependence on observer interpretation [21, 22]. It achieves diagnostic performance comparable to apparent diffusion coefficient (ADC) values in distinguishing cancerous from benign prostate tissue [23-26]. Nonetheless, it is not yet routinely integrated into clinical workflows due to the need for longer acquisition times and additional imaging sequences.

To overcome these constraints, our prior research developed a neural network capable of generating estimated T2 maps retrospectively from standard T1- and T2-weighted images [27]. The current work examines the diagnostic gain of including these estimated T2 maps alongside conventional T2-weighted data for radiomics-based modeling. These models aim to differentiate clinically significant prostate cancer in the peripheral zone (PZ) using combined feature sets.

Materials and Methods

Patient population and data acquisition

This retrospective analysis was approved by the Institutional Review Board of Cedars-Sinai Medical Center, and written consent was obtained from all participants. Between January 2018 and December 2022, biopsy-confirmed peripheral zone lesions were reviewed.

A summary of patient inclusion and exclusion is illustrated in **Figure 1**. In total, 61 patients underwent mpMRI using 3T systems (Biograph mMR; Siemens Healthineers, Erlangen, Germany). MRI acquisition parameters are listed in **Table 1**. All datasets were interpreted by a radiologist with 25 years of prostate imaging experience, in accordance with the PI-RADS v2.1 guidelines [8].

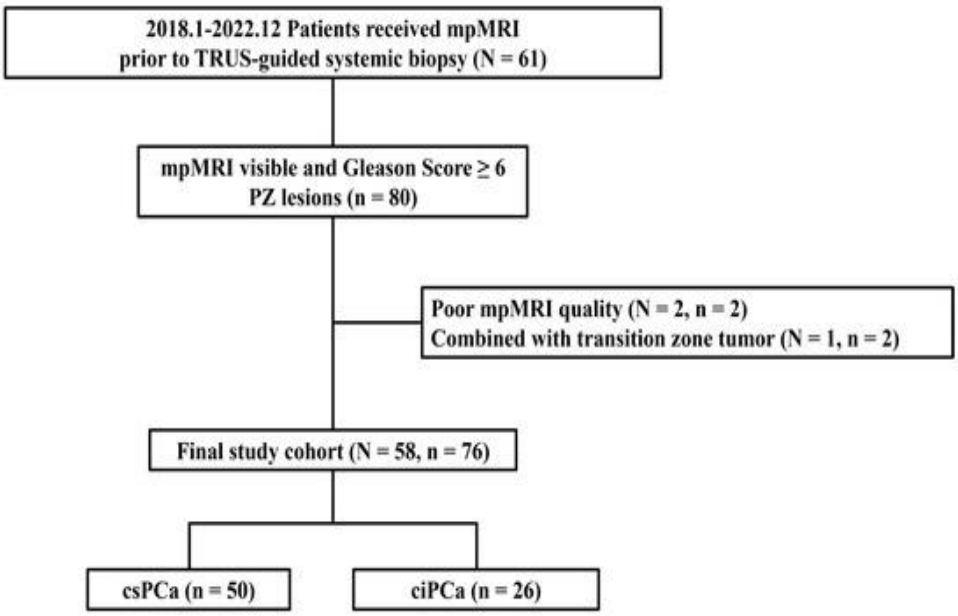

Figure 1. Inclusion and exclusion process of participants. Data from 58 men diagnosed with prostate cancer (PCa), yielding 76 peripheral zone (PZ) lesions, were utilized. The lesions were classified into two outcome groups: 50 were clinically significant prostate cancers (csPCa) and 26 were clinically insignificant cases (ciPCa). Here, N indicates the total number of patients, and n denotes the total lesion count.

Table 1. Overview of imaging acquisition settings for prostate mpMRI scans.

Parameter	T1w (FLASH)	T2w (TSE)	DWI (EPI)	DCE (GRE)
TE (ms)	2.03	132	95	1.07
TR (ms)	277	4000	6500	3.02
Flip angle (°)	65	158	90	10
# Slices	45	30	29	31

Thickness (mm)	6	3	3	3
Resolution (mm²)	1.125 × 1.125	0.63 × 0.63	0.781 × 0.781	1.250 × 1.250
FOV (mm²)	360 × 247.5	160 × 160	200 × 200	160 × 160
Temporal Resolution (s)	/	/	/	20
b-value (s/mm²)	/	/	50, 800, 1400	/
Scan time (min)	0.5	4.5	6.4	8.2

Each subject underwent both a 12-core systematic biopsy guided by TRUS and an MRI-targeted biopsy, localized using a prostate cylindrical coordinate approach [28].
Lesions located in the PZ with a Gleason score of 3 + 4 or higher were labeled as csPCa, whereas lesions scoring 6 were identified as ciPCa.
Exclusion criteria included:
(1) substandard mpMRI quality caused by severe motion or metallic artifacts, and
(2) presence of tumors involving multiple prostate zones, such as those extending into the transition zone. After applying these criteria, 76 lesions from 58 PCa patients remained for analysis. The demographic and clinical information of these participants is presented in **Table 2**.

Table 2. Summary of the clinical profiles of included participants.

Characteristic	Value (Total Patients N = 58, Total Lesions n = 76)
Age (yr), median {IQR}	69 {63.5-73}
PSA (ng/mL), median {IQR}	6.2 {5.1-7.3}
PSAD (ng/mL²), median {IQR}	0.16 {0.09-0.25}
Prostate volume (cc), median {IQR}	41.78 {26.77-58.36}
Gleason Score, n {%}	
3 + 3	26 {34.2}
3 + 4	34 {44.7}
4 + 3	7 {9.2}
≥4 + 4	9 {11.8}
PI-RADS, n {%}	
1	0 {0}
2	0 {0}
3	6 {7.9}
4	47 {61.8}
5	23 {30.3}

Data creation and preprocessing
T2 relaxation maps were generated through a deep learning framework previously developed by our group [27]. The model utilized T1-weighted and T2-weighted images as input data and the reference T2 maps as the training target.
The training cohort included 25 individuals—17 with PCa and 8 healthy controls.
To ensure alignment between input and reference data, the T2-weighted image used during training was reconstructed from multi-echo spin-echo sequences applied for T2 estimation. Both training and inference datasets shared identical echo times. The model configuration and optimization approach followed our earlier publication [27].
A qualified radiologist manually annotated tumor regions of interest (ROIs) on every image slice in both T2-weighted images and T2-derived maps using ITK-SNAP 3.8.0 (www.itksnap.org) [29]. Only PZ lesions that were visible on mpMRI and confirmed positive by biopsy (Gleason ≥ 6) were segmented.

Radiomic analysis

Feature extraction

Each patient's T2-weighted images underwent z-score normalization, while T2 maps generated from the neural network were directly used for analysis.

Figure 2 illustrates the complete analytical workflow designed to build radiomic classifiers for detecting clinically significant PZ cancers based on T2-weighted images and T2-derived maps.

Feature computation was performed on all ROIs using PyRadiomics 3.1.0 (Python 3.7.6), following Image Biomarker Standardization Initiative (IBSI) guidelines [30, 31].

A total of 107 radiomic parameters were derived from each modality, comprising:

- 18 intensity-based features,
- 14 morphological features, and
- 75 texture-derived indices, encompassing GLCM, GLRLM, GLSZM, GLDM, and NGTDM families.

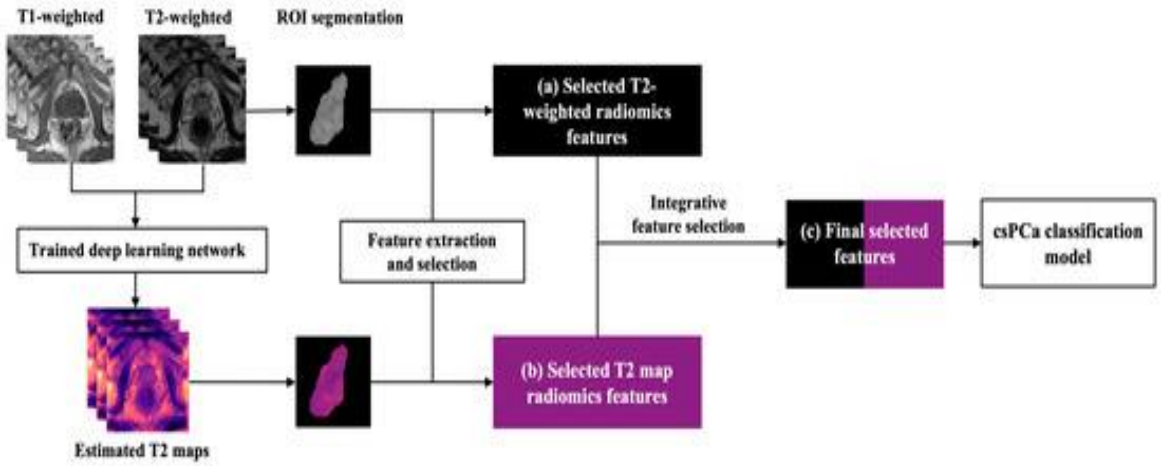

Figure 2. Workflow for radiomic model construction. The deep learning-estimated T2 maps were created from T1- and T2-weighted images. From both modalities, lesion ROIs were processed to obtain radiomic signatures, which were independently filtered and later merged for integrated feature selection. Three sets of predictive models were developed:

(a) models trained on T2-weighted features,
(b) models using T2 map-derived features, and
(c) models combining both feature sets.

Model building

The dataset comprised 76 lesions within the PZ, maintaining an approximate 2:1 ratio between csPCa (n = 50) and ciPCa (n = 26). To correct for this imbalance, the Synthetic Minority Oversampling Technique (SMOTE) was applied. All extracted feature matrices from both imaging types were min-max normalized to a [0, 1] scale. This exploratory investigation assessed whether T2 map-based features added diagnostic value beyond those from T2-weighted imaging. Three feature selection algorithms—Kruskal-Wallis (KW), Relief, and Recursive Feature Elimination (RFE)—were paired with five classifiers: Logistic Regression (LR), Support Vector Machine (SVM), Gaussian Process (GP), LASSO Logistic Regression (LASSO-LR), and Random Forest (RF). Due to the limited dataset size, a 5-fold cross-validation scheme was employed. The area under the ROC curve (AUC) from the validation phase was used to determine the most discriminative features and the optimal selection-classifier pairings.

A grid-search-based procedure was implemented to compare the predictive capability of features obtained from both imaging sources. For each modality, the six best-performing features were initially retained, after which a combined feature subset was created and re-evaluated with the same search process. All computations were executed using FeAture Explorer Pro (FAE v0.5.14) within Python 3.7.6 [32].

Statistical evaluation

Model efficiency was tested through a five-fold cross-validation framework for three feature sets:

(a) T2-weighted feature subset, (b) T2 map-derived features, and (c) combined T2-weighted and T2 map feature sets.

Model performance was assessed via receiver operating characteristic (ROC) curve analysis. Metrics such as accuracy, sensitivity, specificity, positive predictive value (PPV), and negative predictive value (NPV) were determined at the threshold producing the maximum Youden index.

A 95% confidence interval (CI) was estimated using bootstrapping (1000 iterations). The area under the ROC curve (AUC) served as the key indicator of diagnostic performance.

Comparisons between AUCs were carried out through the DeLong statistical test, executed in Python 3.7.6 [33].

Results and Discussion

Selection of radiomic features from T2-weighted images and estimated T2 maps

A total of 76 PZ lesions—comprising 50 clinically significant (csPCa) and 26 clinically insignificant (ciPCa) cases—were used to generate the models using five-fold cross-validation.

Based on the grid-search-based strategy explained earlier, the Kruskal-Wallis (KW) feature selection method combined with a logistic regression (LR) classifier was applied to extract the most discriminative features independently from the T2-weighted and estimated T2 map datasets.

As depicted in **Figure 3**, the KW algorithm ranked all radiomic parameters according to their F-values, considering features statistically relevant at $p < 0.05$.

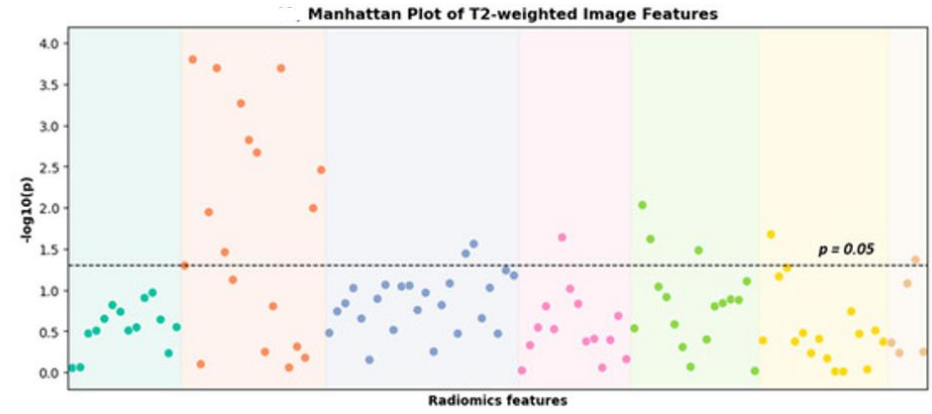

a)

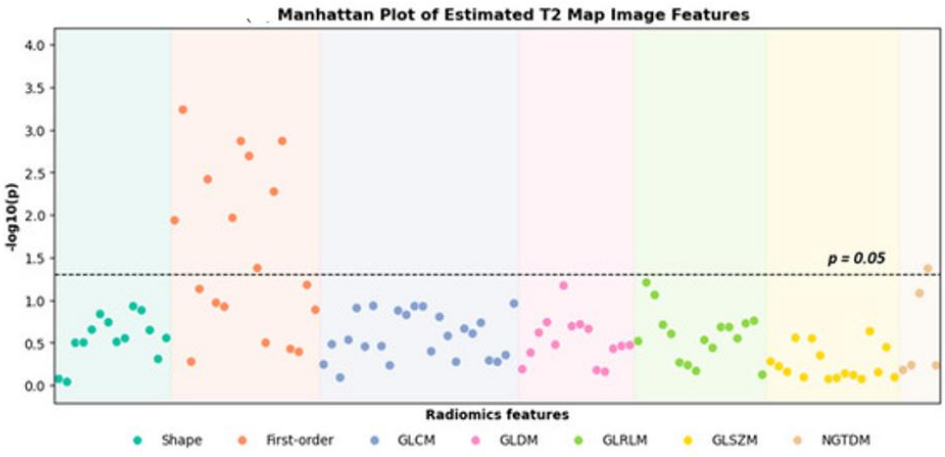

b)

Figure 3. Manhattan plots of all extracted features from (a) T2-weighted images and (b) estimated T2 maps. The plots illustrate p-values across all radiomic variables comparing csPCa and ciPCa groups. The x-axis represents individual features, and the y-axis displays $-\log_{10}(p)$ values. The dashed horizontal line corresponds to the $p = 0.05$ threshold. A total of 18 radiomic parameters from T2-weighted images and 10 from T2 maps exceeded this cutoff and were therefore regarded as statistically significant.

From these, two distinct groups of six key features were selected based on the highest validation AUCs produced by the LR classifiers. **Table 3** outlines these chosen features. For the T2 maps, the six retained parameters were first-order statistics: 10th percentile, 90th percentile, interquartile range, mean, mean absolute deviation, and minimum intensity.

From the T2-weighted data, the selected set comprised two texture measures—GLDM Gray Level Variance and NGTDM Contrast—and four first-order indices—10th percentile, mean, mean absolute deviation, and robust mean absolute deviation. Definitions for these variables are detailed in the PyRadiomics 3.1.0 documentation [31]. For all top-ranked features, values in csPCa lesions were lower than those in ciPCa, with $p < 0.05$ for every comparison.

Table 3. Values of the selected features from T2-weighted images and T2 maps in csPCa and ciPCa groups.

Feature	csPCa	ciPCa	p-Value
T2-Weighted Features			
firstorder_90Percentile	0.44 ± 0.14	0.58 ± 0.15	<0.001 ***
firstorder_MeanAbsoluteDeviation	0.32 ± 0.17	0.48 ± 0.18	<0.001 ***
firstorder_RobustMeanAbsoluteDeviation	0.31 ± 0.18	0.49 ± 0.21	<0.001 ***
firstorder_Mean	0.46 ± 0.15	0.58 ± 0.17	<0.01 **
gldm_GrayLevelVariance	0.30 ± 0.19	0.41 ± 0.19	0.02 *
ngtdm_Contrast	0.20 ± 0.17	0.29 ± 0.16	0.04 *
Estimated T2 Map Features			
firstorder_90Percentile	0.40 ± 0.15	0.53 ± 0.16	<0.001 ***
firstorder_InterquartileRange	0.25 ± 0.15	0.36 ± 0.14	<0.01 **
firstorder_Mean	0.38 ± 0.15	0.51 ± 0.16	<0.01 **
firstorder_10Percentile	0.32 ± 0.16	0.43 ± 0.19	0.01 *
firstorder_MeanAbsoluteDeviation	0.29 ± 0.16	0.38 ± 0.13	0.01 *
firstorder_Minimum	0.31 ± 0.23	0.43 ± 0.22	0.04 *

Highlighted rows represent variables used in constructing the combined model.
*Significance codes: *p < 0.05; **p < 0.01; **p < 0.001.

Performance results of LR classifiers for each feature category are listed in **Table 4**, with corresponding ROC curves for PZ csPCa detection.

The T2-weighted model achieved an AUC of 0.700 (95% CI: 0.568-0.831), with accuracy 0.737, sensitivity 0.800, specificity 0.615, PPV 0.800, and NPV 0.615.

The model based on T2 map features achieved an AUC of 0.763 (95% CI: 0.649-0.877), accuracy 0.711, sensitivity 0.640, specificity 0.846, PPV 0.890, and NPV 0.550.

This reflected a relative AUC increase of 6.3%, though no statistically significant difference was found between the two (DeLong test).

Table 4. Comparison of prediction performance across models using T2-weighted, T2 map, and integrative feature sets. p-values are derived from DeLong tests comparing AUCs of T2 map-based and integrative models against the T2-weighted baseline.

	AUC	95% CIs	ACC	SEN	SPE	PPV	NPV	p-Value
T2-weighted image	0.700	[0.568-0.831]	0.737	0.800	0.615	0.800	0.615	/
Estimated T2 map	0.763	[0.649-0.877]	0.711	0.640	0.846	0.890	0.550	0.260
T2 weighted + Estimated T2 map	0.803	[0.694-0.913]	0.803	0.780	0.846	0.907	0.667	0.043 *

*Significance: $p < 0.05$.

Development of the integrative model

Feature integration was carried out by combining 12 preselected variables—six from each modality—into a single pool.

Applying the same grid-search strategy, nine final predictors were identified through the Relief selection

algorithm coupled with a Gaussian Process (GP) classifier. As summarized in **Table 3**, all six T2 map features remained within this final subset, while three from the T2-weighted group—one texture feature (GLDM Gray Level Variance) and two first-order indices (Mean Absolute Deviation and Robust Mean Absolute Deviation)—were also retained.

Figure 4 displays representative classification examples:

(A) a correctly predicted ciPCa lesion and
(B) a correctly predicted csPCa lesion in the PZ.

(B) The visual comparison of the selected discriminative features indicates a distinct trend—csPCa lesions consistently show lower feature values relative to ciPCa.

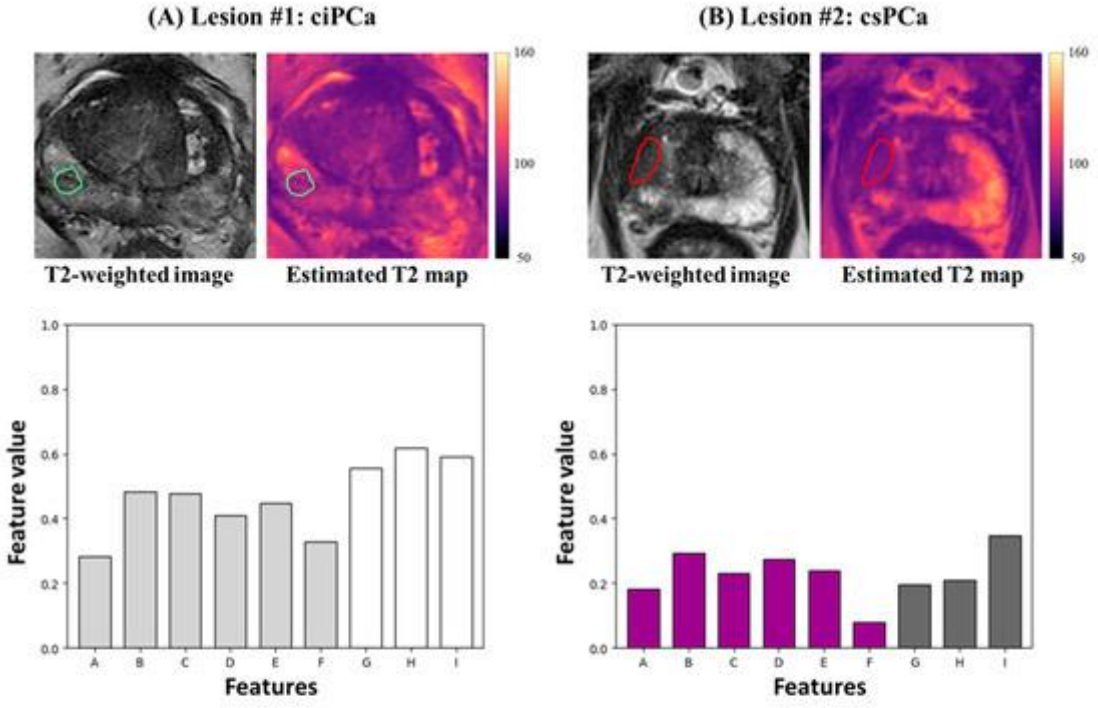

Integrative selected features		Index
Estimated T2 map	t2map_firstorder_10Percentile	A
	t2map_firstorder_90Percentile	B
	t2map_firstorder_InterquartileRange	C
	t2map_firstorder_Mean	D
	t2map_firstorder_MeanAbsoluteDeviation	E
	t2map_firstorder_Minimum	F
T2-weighted image	t2w_firstorder_MeanAbsoluteDeviation	G
	t2w_firstorder_RobustMeanAbsoluteDeviation	H
	t2w_gldm_GrayLevelVariance	I

Figure 4. Illustration of T2-weighted imaging, reconstructed T2 maps, and integrative predictive feature values for two correctly identified lesion examples.

(a) presents a PZ ciPCa case, where the lesion ROI is traced in green on both the T2-weighted scan and its corresponding estimated T2 map ([ms]) for the same section. The histogram displays the feature measurements—light gray columns indicate those obtained from the T2 map, while white columns denote those from the T2-weighted image.

(b) shows a PZ csPCa case, the ROI outlined in red. Here, purple bars correspond to T2 map features, and dark gray bars represent T2-weighted image features. The index numbers in the table below align with the histogram's x-axis values.

Using the final nine most discriminative features, model performance yielded the following results: AUC = 0.803 (95% CI: 0.694-0.913), accuracy = 0.803, sensitivity = 0.780, specificity = 0.846, PPV = 0.907, and NPV = 0.667.

As detailed in **Table 4** and **Figure 5**, this combined model increased AUC by 10.3% and 3.7% compared to those relying solely on T2-weighted or T2-map features. The comparison between the integrative model and the T2-weighted model showed statistical significance ($p = 0.048$).

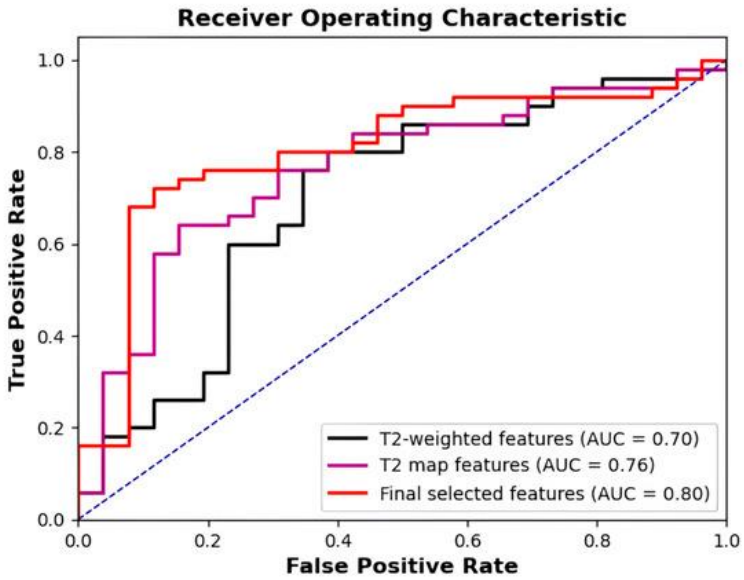

Figure 5. ROC curves of the radiomics classifiers built on (1) selected T2-weighted features (black), (2) selected T2-map features (purple), and (3) the combined T2-weighted plus T2-map features (red). The validation AUC values were 0.700, 0.763, and 0.803, respectively.

This investigation established radiomic classifiers for predicting PZ csPCa using parameters derived from both T2-weighted scans and computed T2 maps. Combining the optimized features from the two imaging types markedly enhanced predictive capability compared with models that depended only on T2-weighted imaging. These results emphasize the contribution of quantitative radiomic parameters obtained from estimated T2 maps.

Prostate tumor diagnosis and surveillance often depend on repeat biopsy procedures; however, radiomic assessment based on MRI is emerging as a promising non-invasive alternative for evaluating tumor behavior. Among mpMRI sequences, T2-weighted imaging provides superior spatial detail and strong tissue contrast—fundamental aspects for radiomics. Yet, unlike ADC maps generated from diffusion-weighted imaging (DWI), T2-weighted scans lack quantitative information since their signal intensity reflects only relative contrast, which varies with acquisition parameters and RF uniformity. To reduce such inconsistencies, normalization procedures such as mean- or z-score-based correction are generally applied. Other techniques use a pair of reference tissue intensities to normalize T2W images and form pseudo-T2 maps [34, 35]; however, these require manual reference segmentation and may produce inconsistent T2 estimations depending on tissue pair selection.

T2 mapping, in contrast, delivers reproducible quantitative T2 metrics directly linked to tumor aggressiveness [24, 36]. To exploit this benefit, we retrospectively generated estimated T2 maps without extra scan time or sequence adjustments. Six first-order texture metrics extracted from these maps contributed to the final integrated classifier, describing the distribution of voxel intensities within tumor ROIs and encapsulating the quantitative strength of T2 analysis. Tumors with intermediate-to-high-grade PCa displayed significantly lower T2 values than low-grade tumors, consistent with the selected T2-map feature profiles.

While DWI and ADC are key mpMRI elements widely used for assessing prostate cancer aggressiveness [17, 37, 38], these modalities were not included here, as our goal was to isolate and assess the impact of T2-derived radiomics alone. The dataset showed substantial alignment discrepancies between T2-weighted/T2-map images and DWI/ADC data due to protocol variations, spatial-resolution differences, distortion in DWI, and bladder-size fluctuations. These inconsistencies would compromise the regional correspondence required for reliable feature fusion in radiomics analysis. Even so, combining DWI and ADC characteristics could further improve model accuracy once image-registration issues—particularly in pelvic imaging—are addressed. Future work employing advanced registration techniques may enable fully integrated multiparametric radiomic evaluation for enhanced prostate cancer stratification.

T2-weighted imaging, although qualitative, provides superior spatial resolution and tissue-specific contrast, making its texture-based characteristics highly informative for evaluating prostate cancer (PCa) aggressiveness. Prior investigations have indicated that texture metrics reflecting tissue uniformity on T2-weighted scans correlate positively with the Gleason Score of prostate cancer [39, 40]. In this research, three radiomic variables from T2-weighted images were incorporated into the final predictive model—one GLDM-derived textural parameter (Gray Level Variance) and two first-order statistical measures (Mean Absolute Deviation and Robust Mean Absolute Deviation). Comparative analysis revealed that csPCa lesions exhibited significantly lower values for both variance and deviation compared to non-significant lesions. This observation aligns with earlier findings indicating that high-grade tumors display greater internal uniformity than low-grade ones. From a pathological perspective, varying degrees of prostate cancer severity are associated with distinct alterations in intracellular makeup, fluid concentration, collagen density, and fibromuscular stroma. High-grade PCa typically shows poor differentiation, high cell density, and limited extracellular space, whereas lower-grade malignancies retain some glandular organization, maintaining intercellular spacing [17, 41]. The selected T2-weighted features in this model emphasize that tumor homogeneity serves as a crucial indicator for enhancing radiomics-based evaluation of PCa severity.

The final integrative model combined six radiomic features derived from the estimated T2 maps with three features extracted from T2-weighted scans. The quantitative characteristics of the T2 maps contributed intensity-based insights, while the qualitative T2-weighted data added variance-related information through first-order and texture descriptors. The fusion of these complementary inputs led to a significant enhancement in the predictive capacity of the PZ PCa model compared to T2-weighted features alone. These outcomes reaffirm the diagnostic benefit of retrospectively computed T2 maps for non-invasive prostate cancer evaluation. Because the estimated T2 maps were generated retrospectively from routinely acquired T1- and T2-weighted sequences, this method can be implemented in existing clinical workflows without modification. The established model can operate as an auxiliary decision-support system within radiology practice, providing reproducible and objective quantitative information.

Several limitations must be acknowledged. First, as discussed earlier, DWI and ADC data were omitted due to the study's emphasis on assessing the contribution of the estimated T2 maps and the technical difficulties caused by image misalignment. Second, the investigation exclusively analyzed clinically significant PCa located within the peripheral zone (PZ). No radiomic features or models were developed for tumors arising in other prostate regions. PZ lesions constitute approximately 70-75% of prostate cancers and typically display broader T2 value ranges for both normal and cancerous tissues compared with non-PZ regions [8, 22, 36]. Furthermore, radiomics literature indicates that feature relevance for tumor detection differs across zones [42]. Therefore, this research focused solely on PZ lesions to assess the diagnostic value of quantitative data derived from the estimated T2 maps. Third, the dataset included 76 cases obtained from a single institution using a standardized mpMRI protocol on the same scanner. Given this limited sample size, a 5-fold cross-validation method was applied rather than a separate test cohort, and the incremental benefit of the estimated T2 map features was quantified through validation AUC metrics. Future research should aim to construct independent models tailored for evaluating lesions in all three prostate zones and should integrate DWI, ADC, and DCE sequences once alignment issues are resolved. The reproducibility and generalizability of the identified radiomic parameters also require verification using larger, multi-institutional datasets.

Conclusion

This work demonstrated that radiomics models incorporating deep learning-generated T2 maps enhance the detection of csPCa within the peripheral zone. Combining information from conventional qualitative T2-weighted imaging with retrospectively derived quantitative T2 maps significantly increased predictive performance compared to T2-weighted imaging alone. The radiomic signatures extracted from estimated T2 maps contributed additional quantitative insight, improving patient risk stratification. Overall, these findings highlight the promise of retrospective T2 mapping as an effective adjunct in precision diagnosis and personalized management of prostate cancer.

Acknowledgments: None

Conflict of Interest: None

Financial Support: None

Ethics Statement: None

References

1. Siegel RL, Giaquinto AN, Jemal A. Cancer Statistics, 2024. CA Cancer J Clin. 2024;74(1):12–49.
2. American Cancer Society. Cancer Facts & Figures 2024. Atlanta: Am Cancer Soc.; 2024.
3. EAU Guidelines. Edn. Presented at the EAU Annual Congress Paris 2024; EAU Guidelines Office: Arnhem, The Netherlands; 2024. ISBN 978-94-92671-23-3.
4. Stephan C, Rittenhouse H, Hu X, Cammann H, Jung K. Prostate-Specific Antigen (PSA) Screening and New Biomarkers for Prostate Cancer (PCa). EJIFCC. 2014;25(1):55–78.
5. Descotes JL. Diagnosis of Prostate Cancer. Asian J Urol. 2019;6(2):129–36.
6. Loeb S, Vellekoop A, Ahmed HU, Catto J, Emberton M, Nam R, et al. Systematic Review of Complications of Prostate Biopsy. Eur Urol. 2013;64(6):876–92.
7. Abraham NE, Mendhiratta N, Taneja SS. Patterns of Repeat Prostate Biopsy in Contemporary Clinical Practice. J Urol. 2015;193(4):1178–84.
8. Turkbey B, Rosenkrantz AB, Haider MA, Padhani AR, Villeirs G, Macura KJ, et al. Prostate Imaging Reporting and Data System Version 2.1: 2019 Update of Prostate Imaging Reporting and Data System Version 2. Eur Urol. 2019;76(3):340–51.
9. Ahmed HU, El-Shater Bosaily A, Brown LC, Gabe R, Kaplan R, Parmar MK, et al. Diagnostic Accuracy of Multi-Parametric MRI and TRUS Biopsy in Prostate Cancer (PROMIS): A Paired Validating Confirmatory Study. Lancet. 2017;389(10071):815–22.
10. Thompson JE, van Leeuwen PJ, Moses D, Shnier R, Brenner P, Delprado W, et al. The Diagnostic Performance of Multiparametric Magnetic Resonance Imaging to Detect Significant Prostate Cancer. J Urol. 2016;195(5):1428–35.
11. Yakar D, Debats OA, Bomers JGR, Schouten MG, Vos PC, van Lin E, et al. Predictive Value of MRI in the Localization, Staging, Volume Estimation, Assessment of Aggressiveness, and Guidance of Radiotherapy and Biopsies in Prostate Cancer. J Magn Reson Imaging. 2012;35(1):20–31.
12. Fütterer JJ, Briganti A, De Visschere P, Emberton M, Giannarini G, Kirkham A, et al. Can Clinically Significant Prostate Cancer Be Detected with Multiparametric Magnetic Resonance Imaging? A Systematic Review of the Literature. Eur Urol. 2015;68(6):1045–53.
13. Rosenkrantz AB, Ginocchio LA, Cornfeld D, Froemming AT, Gupta RT, Turkbey B, et al. Interobserver Reproducibility of the PI-RADS Version 2 Lexicon: A Multicenter Study of Six Experienced Prostate Radiologists. Radiology. 2016;280(3):793–804.
14. Greer MD, Shih JH, Lay N, Barrett T, Bittencourt L, Borofsky S, et al. Interreader Variability of Prostate Imaging Reporting and Data System Version 2 in Detecting and Assessing Prostate Cancer Lesions at Prostate MRI. AJR Am J Roentgenol. 2019;212(5):1197–205.
15. Gillies RJ, Kinahan PE, Hricak H. Radiomics: Images Are More than Pictures, They Are Data. Radiology. 2016;278(2):563–77.
16. Lambin P, Leijenaar RTH, Deist TM, Peerlings J, de Jong EEC, van Timmeren J, et al. Radiomics: The Bridge between Medical Imaging and Personalized Medicine. Nat Rev Clin Oncol. 2017;14(12):749–62.
17. Chen T, Li M, Gu Y, Zhang Y, Yang S, Wei C, et al. Prostate Cancer Differentiation and Aggressiveness: Assessment With a Radiomic-Based Model vs. PI-RADS V2. J Magn Reson Imaging. 2019;49(3):875–84.
18. Toivonen J, Montoya Perez I, Movahedi P, Merisaari H, Pesola M, Taimen P, et al. Radiomics and Machine Learning of Multisequence Multiparametric Prostate MRI: Towards Improved Non-Invasive Prostate Cancer Characterization. PLoS ONE. 2019;14(5):e0217702.
19. Min X, Li M, Dong D, Feng Z, Zhang P, Ke Z, et al. Multi-Parametric MRI-Based Radiomics Signature for Discriminating between Clinically Significant and Insignificant Prostate Cancer: Cross-Validation of a Machine Learning Method. Eur J Radiol. 2019;115:16–21.

20. Hectors SJ, Cherny M, Yadav KK, Beksaç AT, Thulasidass H, Lewis S, et al. Radiomics Features Measured with Multiparametric Magnetic Resonance Imaging Predict Prostate Cancer Aggressiveness. J Urol. 2019;202(3):498–505.
21. Liu W, Turkbey B, Sénégas J, Remmele S, Xu S, Kruecker J, et al. Accelerated T2 Mapping for Characterization of Prostate Cancer. Magn Reson Med. 2011;65(5):1400–6.
22. Hoang Dinh A, Souchon R, Melodelima C, Bratan F, Mège-Lechevallier F, Colombel M, et al. Characterization of Prostate Cancer Using T2 Mapping at 3T: A Multi-Scanner Study. Diagn Interv Imaging. 2015;96(4):365–72.
23. Panda A, O'Connor G, Lo WC, Jiang Y, Margevicius S, Schluchter M, et al. Targeted Biopsy Validation of Peripheral Zone Prostate Cancer Characterization With Magnetic Resonance Fingerprinting and Diffusion Mapping. Invest Radiol. 2019;54(8):485–93.
24. Hepp T, Kalmbach L, Kolb M, Martirosian P, Hilbert T, Thaiss WM, et al. T2 Mapping for the Characterization of Prostate Lesions. World J Urol. 2022;40(6):1455–61.
25. Chatterjee A, Devaraj A, Mathew M, Szasz T, Antic T, Karczmar GS, et al. Performance of T2 Maps in the Detection of Prostate Cancer. Acad Radiol. 2019;26(1):15–21.
26. Langer DL, van der Kwast TH, Evans AJ, Plotkin A, Trachtenberg J, Wilson BC, et al. Prostate Tissue Composition and MR Measurements: Investigating the Relationships between ADC, T2, Ktrans, ve, and Corresponding Histologic Features. Radiology. 2010;255(2):485–94.
27. Sun H, Wang L, Daskivich T, Qiu S, Han F, D'Agnolo A, et al. Retrospective T2 Quantification from Conventional Weighted MRI of the Prostate Based on Deep Learning. Front Radiol. 2023;3:1223377.
28. Patel DN, Nguyen C, Sirohi D, Falahatian V, Saouaf R, Luthringer D, et al. Use of Cylindrical Coordinates to Localize Prostate Cancers on MRI and Prostatectomy Pathology. Urol Oncol Semin Orig Investig. 2017;35(9):673.e15–e20.
29. Yushkevich PA, Piven J, Hazlett HC, Smith RG, Ho S, Gee JC, et al. User-Guided 3D Active Contour Segmentation of Anatomical Structures: Significantly Improved Efficiency and Reliability. Neuroimage. 2006;31(3):1116–28.
30. Zwanenburg A, Vallières M, Abdalah MA, Aerts HJW, Andrearczyk V, Apte A, et al. The Image Biomarker Standardization Initiative: Standardized Quantitative Radiomics for High-Throughput Image-Based Phenotyping. Radiology. 2020;295(2):328–38.
31. van Griethuysen JJ, Fedorov A, Parmar C, Hosny A, Aucoin N, Narayan V, et al. Computational Radiomics System to Decode the Radiographic Phenotype. Cancer Res. 2017;77(21):e104–e107.
32. Song Y, Zhang J, Zhang Y, Hou Y, Yan X, Wang Y, et al. FeAture Explorer (FAE): A Tool for Developing and Comparing Radiomics Models. PLoS ONE. 2020;15(6):e0237587.
33. DeLong ER, DeLong DM, Clarke-Pearson DL. Comparing the Areas under Two or More Correlated Receiver Operating Characteristic Curves: A Nonparametric Approach. Biometrics. 1988;44(3):837–45.
34. Sunoqrot MRS, Nketiah GA, Selnæs KM, Bathen TF, Elschot M. Automated Reference Tissue Normalization of T2-Weighted MR Images of the Prostate Using Object Recognition. Magn Reson Mater Phys Biol Med. 2021;34(3):309–21.
35. Sørland KI, Sunoqrot MRS, Sandsmark E, Langørgen S, Bertilsson H, Trimble CG, et al. Pseudo-T2 Mapping for Normalization of T2-Weighted Prostate MRI. Magn Reson Mater Phys Biol Med. 2022;35(2):573–85.
36. Klingebiel M, Schimmöller L, Weiland E, Franiel T, Jannusch K, Kirchner J, et al. Value of T2 Mapping MRI for Prostate Cancer Detection and Classification. J Magn Reson Imaging. 2022;56(2):413–22.
37. Bonekamp D, Kohl S, Wiesenfarth M, Schelb P, Radtke JP, Götz M, et al. Radiomic Machine Learning for Characterization of Prostate Lesions with MRI: Comparison to ADC Values. Radiology. 2018;289(1):128–37.
38. Itou Y, Nakanishi K, Narumi Y, Nishizawa Y, Tsukuma H. Clinical Utility of Apparent Diffusion Coefficient (ADC) Values in Patients with Prostate Cancer: Can ADC Values Contribute to Assess the Aggressiveness of Prostate Cancer? J Magn Reson Imaging. 2011;33(1):167–72.
39. Wibmer A, Hricak H, Gondo T, Matsumoto K, Veeraraghavan H, Fehr D, et al. Haralick Texture Analysis of Prostate MRI: Utility for Differentiating Non-Cancerous Prostate from Prostate Cancer and Differentiating Prostate Cancers with Different Gleason Scores. Eur Radiol. 2015;25(9):2840–50.

40. Vignati A, Mazzetti S, Giannini V, Russo F, Bollito E, Porpiglia F, et al. Texture Features on T2-Weighted Magnetic Resonance Imaging: New Potential Biomarkers for Prostate Cancer Aggressiveness. Phys Med Biol. 2015;60(7):2685–701.
41. Hegde JV, Mulkern RV, Panych LP, Fennessy FM, Fedorov A, Maier SE, et al. Multiparametric MRI of Prostate Cancer: An Update on State-of-the-Art Techniques and Their Performance in Detecting and Localizing Prostate Cancer. J Magn Reson Imaging. 2013;37(5):1035–54.
42. Ginsburg SB, Algohary A, Pahwa S, Gulani V, Ponsky L, Aronen HJ, et al. Radiomic Features for Prostate Cancer Detection on MRI Differ Between the Transition and Peripheral Zones: Preliminary Findings from a Multi-Institutional Study. J Magn Reson Imaging. 2017;46(1):184–93.